Calorimetric Study: Surface Energetics and the Magnetic Transition in Nanocrystalline CoO

Lan Wang,[†] Kiem Vu,[†] Alexandra Navrotsky,*[,†] Rebecca Stevens,[‡] Brian F. Woodfield,[‡] and Juliana Boerio-Goates[‡]

Thermochemistry Facility and NEAT ORU, University of California at Davis, Davis, California 95616, and Department of Chemistry and Biochemistry, Brigham Young University, Provo, Utah 84602

Received June 15, 2004. Revised Manuscript Received September 23, 2004

CoO nanoparticles ranging in size from 7 to 21 nm were prepared via precipitation and thermal decomposition methods. The particles had water contents ranging from 2.18 to 0.19 wt %; water content decreased with increasing particle size. All particles also contained a small amount of Co_3O_4 impurity. The surface enthalpy was determined to be 2.82 ± 0.20 $J \cdot m^{-2}$ by acid solution calorimetry at 298 K. Corrections were made for the water and cobalt spinel impurity. Heat capacity measurements using adiabatic (10−320 K) and semi-adiabatic (0.6−40 K) calorimeters were performed on the sample with particle size 7.0 ± 1.0 nm. The nanoparticle heat capacity had a broad anomaly with a rounded maximum at 265 K, a reduction of 23 K from the Néel temperature T_N observed as a sharply peaked maximum in the heat capacity of single-crystal CoO. When corrected for water and Co_3O_4, the heat capacity of nanophase CoO is greater than that of single-crystal CoO below about 250 K. Above 250 K, the much larger magnetic peak in the heat capacity of the single crystal dominates the heat capacity difference. Thus the excess entropy of the nanoparticles, calculated from the heat capacity difference, has a maximum of 2.4 ± 0.3 $J \cdot K^{-1} \cdot mol^{-1}$ at 245 K but drops to 1.5 ± 0.3 $J \cdot K^{-1} \cdot mol^{-1}$ at 298 K. The magnetic and surface contributions to the excess entropy cannot be resolved in a definitive manner, but an estimate of the surface entropy, 0.28 ± 0.03 $mJ \cdot K^{-1} \cdot m^{-2}$, is similar to one literature report for MgO, and the excess magnetic entropy is negative, −0.8 ± 0.3 $J \cdot K^{-1} \cdot mol^{-1}$.

Introduction

Bulk CoO has been investigated for many years both in fundamental research and in technological applications.[1−6] Because the vibrational, electronic, and magnetic properties of materials at the nanoscale can be strikingly different from those in the bulk, there is the potential for new magnetic properties and catalytic activity, so nanoparticles of CoO nanoparticles have been of increasing interest.[7−13] For example, it has been reported that the Néel temperature (T_N) decreases with size for particles in the size range of 2.0−3.0 nm by ESR measurement.[9] However, no significant T_N shifts were observed in hysteresis loop curves for particles ranging from 10 to 80 nm.[12]

Thermodynamic properties, such as the enthalpy of formation and the entropy, of small particles can differ significantly from those of the bulk, even leading to crossovers in phase stability of nanophases compared to bulk phases.[14] It is customary to attribute these differences to surface effects, and a surface free energy can be defined in term of surface enthalpy and entropy:[14−19]

$$G_{surface}\ (J \cdot m^{-2}) = H_{surface}\ (J \cdot m^{-2}) - TS_{surface}\ (J \cdot m^{-2} \cdot K^{-1}) \quad (1)$$

The surface enthalpy can be measured directly via solution calorimetry,[14,20−22] while the entropy term can

* Corresponding author. Tel: (530)-752-3292. Fax: (530)-752-9307. E-mail: anavrotsky@ucdavis.edu.
† University of California at Davis.
‡ Brigham Young University.

(1) Jauch, W.; Reehuis, M; Bleif, H. J.; Kubanek, F. *Phys. Rev. B* **2001**, *64*, 052102.
(2) Chen, M.; Hallstedt, B.; Gauckler, L. J. *J. Phase Equilib.* **2003**, *24*, 212.
(3) Kuznetsov, V. I.; Sadykov, V. A.; Razdobarov, V. A.; Klimenko, A. G. *J. Solid State Chem.* **1993**, *104*, 412.
(4) Grimes, R. W.; Lagerlöf, K. P. D. *J. Am. Ceram. Soc*. **1991**, *74*, 270.
(5) Redman, M. J.; Steward, E. G. *Nature* **1962**, *193*, 867.
(6) DiCarlo, J.; Navrotsky, A. *J. Am. Ceram. Soc.* **1993**, *76*, 2465.
(7) Verelst, M.; Ely, T. O.; Amiens, C.; Snoeck, E.; Lecante, P.; Mosset, A.; Respaud, M.; Broto, J. M.; Chaudret, B. *Chem. Mater*. **1999**, *11*, 2702.
(8) Yin, J. S.; Wang, Z. L. *Phys. Rev. Lett*. **1997**, *79*, 2570.
(9) Sako, S.; Ohshima, K.; Sakai, M.; Bandow, S. *Surf. Rev. Lett*. **1996**, *3*, 109.
(10) Flipse, C. F. J.; Rouwelaar, C. B.; Groot, F. M. F. *Eur. Phys. J. D* **1999**, *9*, 479.
(11) Soriano, L.; Abbate, M.; Fernández, A.; González-Elipe, A. R.; Sirotti, F.; Sanz, J. M. *J. Phys. Chem. B* **1999**, *103*, 6676.
(12) Zhang, L.; Xue, D.; Gao, C. *J. Magn. Magn. Mater*. **2003**, *267*, 111.
(13) Guo, L.; Wu, B.; Zhuang, Y.; Li, Q.; Zhu, H. *Huanjing Kexue Xuebao* **1998**, *18*, 457.
(14) Navrotsky, A. *Geochem. Trans.* **2003**, *4*, 34.
(15) Zhang, H.; Gilbert, B.; Huang, F.; Banfield, J. F. *Nature* **2003**, *424*, 1025.
(16) Hill, T. L. *Nano Lett.* **2001**, *1*, 273.
(17) Nanda, K. K.; Maisels, A.; Kruis, F. E.; Fissan, H.; Stappert, S. *Phys. Rev. Lett*. **2003**, *91*, 106102.
(18) Zhang, H.; Penn, R. L.; Hamers, R. J.; Banfield, J. F. *J. Phys. Chem. B* **1999**, *103*, 4656.

10.1021/cm049040i CCC: $27.50
Published on Web 11/12/2004

be obtained from an integration of the excess heat capacity in adiabatic calorimetry measurements from 0 to 298.15 K.[23−25]

The heat capacity itself is a very sensitive probe of magnetic and vibrational phenomena, and quantitative differences between the nanoparticles and bulk material can be obtained with high accuracy. Experimental evidence and computer simulations show the heat capacities of nanoparticles are greater than those of the polycrystalline bulk; the magnitude of the excess heat capacity (C_{ex}) is temperature and particle-size dependent.[26−30] Two characteristic features have been observed. For materials that have been measured to very low temperatures (primarily metals), the heat capacity exhibits a linear temperature dependence (γ_{ex}) that is in excess of the bulk value.[27,30] At temperatures above 20 K, C_{ex} appears to go through a maximum.[26,28] However, no nanophase heat capacities have been studied over a wide enough temperature range or on well-characterized materials to explore whether both features are present simultaneously and whether γ_{ex} has a phonon or electronic origin.

The purpose of the present research is to investigate the surface energy of CoO nanoparticles with solution calorimetry, and heat capacity and magnetic properties by adiabatic calorimetry over a wide temperature range.

Experimental Section

Synthesis. CoO nanoparticles were prepared by thermal decomposition of cobalt hydroxides in a hydrogen/argon mixture atmosphere. Briefly, 10.0 mL of 1.0 M aqueous cobalt nitrate solution (Fluka, $Co(NO_3)_6 \cdot H_2O$, >99.0%) was added into 50.0 mL of 0.5 M ammoniacal solution in a three-necked round-bottom flask in 15 s. The ammoniacal solution was bubbled with argon at a flow rate of 10 mL·min^{-1} at room temperature for 30 min to remove dissolved oxygen before the Co^{2+} nitrate was added. The addition and precipitation were carried out while the mixture was stirred under an atmosphere of argon. After aging for 5 min, the precipitate was filtered with a vacuum filter, washed with deionized water until the wash water was neutral in pH, and then dried in a vacuum desiccator at room temperature overnight. CoO nanoparticles were synthesized by heating the dry precipitate at fixed temperatures (350, 400, 450, and 500 °C) for 2 h under a flowing H_2/Ar mixture (1% H_2 by volume, flow rate of 60 mL·min^{-1}). Following synthesis, the CoO nanoparticles were stored in a glovebox under an argon atmosphere. The preparation of bulk CoO from Co_3O_4 has been reported previously;[23] a single crystal with original dimensions of approximately 27 mm × 18 mm × 1 mm, prepared commercially (Commercial Crystal Labs, 4406 Arnold Avenue, Naples, FL 34104, www.crystalguru.com), was broken into pieces of several mm on an edge and 1 mm thick for the heat capacity measurements.

Characterization. XRD patterns were collected using a Scintag PAD V diffractometer (Cu Kα radiation, 45 kV, 40 mA, and $\theta-2\theta$ goniometer geometry) in a step-scan mode with steps of 0.02° and dwell time of 10 s. The patterns were analyzed using commercial software.[31] The specific surface areas were measured by the multipoint Brunauer−Emmett−Teller (BET) method with a Micromeritics 2020 accelerated surface area and porosimetry system (ASAP). Measurements were performed in a liquid nitrogen bath, with N_2 as the adsorbate gas. A 100-mg sample was loaded into a glass tube and degassed in a vacuum of 10^{-3} Torr overnight before the measurements. Particle size and morphology were studied by scanning and transmission electron microscopy, using a FEI XL30-SFEG high-resolution SEM and Topcon 002b TEM. The samples were dispersed in ethanol by ultrasound and dropped on a copper grid with a carbon film for TEM or an aluminum peg with a flat surface for SEM. Water and excess oxygen contents were measured by thermogravimetry (TGA) with a Netzch 449 simultaneous thermal analyzer (STA) apparatus in an argon atmosphere, with a heating rate of 10 °C·min^{-1}. The concentrations of trace metals were investigated using electron microprobe analysis on a Cameca SX-100 instrument.

Enthalpy of Solution. The solution calorimetry was performed on a Calorimetry Sciences Corporation (CSC) isothermal microcalorimeter (IMC) 4400 modified to allow experiments with corrosive solutions. The calorimetric experiments consisted of dropping a pelletized sample of nano-CoO (5 mg) into 25.00 g of hydrochloric (5.0 N) acid at 25.00 °C in a liquid bath. The samples dissolved quickly under smooth mechanical stirring and no calorimetric difficulties were encountered. The apparatus was calibrated using measurements of the enthalpy of solution of potassium chloride (NIST SRM 999) in deionized water.

Heat Capacity. The constant pressure heat capacity, C_p, was measured using two different calorimeters. Measurements were made from 10 to 320 K in a home-built adiabatic calorimeter of the Westrum design that has been described previously.[24] The calorimetric accuracy has been tested by C_p measurements of α-Al_2O_3 (NIST SRM 720) and a high-purity copper sample over the region $15 < T/K < 400$. Below 15 K deviations from the literature values were ±2% near $T = 15$ K; the deviations decreased systematically to ±0.15% at $T = 50$ K and were within ±0.15% in the region $50 < T/K < 400$. For the nano and bulk CoO experiments, approximately 6 g of material was pelletized and loaded into a gold-plated copper vessel for the measurement. The pelletizing and loading process was conducted in an argon-filled glovebox with water and oxygen contents below 1 ppm. Measurements were made from 0.6 to 60 K using pulsed techniques in a semi-adiabatic calorimeter described in detail elsewhere.[25] During the loading of the low-temperature apparatus, the sample was exposed to the atmosphere for less than 10 min. The accuracy of the heat capacity data as measured on that apparatus is generally better than ±0.25% with a precision better than ±0.1% on samples with good thermal conductivity. On insulators such as the samples here, the accuracy is reduced somewhat above 20 K because of long thermal relaxation times. The data sets from the two experiments are combined into a single set by choosing a temperature in the overlap region where there is agreement of the heat capacities and a smooth variation in the first and second derivatives about the join.

Results and Discussion

Crystallite Size, Surface Area, and Composition of CoO Nanoparticles. XRD patterns of CoO nano-

(19) Navrotsky, A. In *Nanoparticles and the Environment*; Banfield, J. F., Navrotsky, A., Eds; Vol. 44 of Reviews in Mineralogy and Geochemistry; Mineralogical Society of America: Washington, DC, 2001; p 73.
(20) McHale, J. M.; Auroux, A.; Perrotta, A. J.; Navrotsky, A. *Science* **1997**, *277*, 788.
(21) Ranade, M. R.; Navrotsky, A.; Zhang, H. Z.; Banfield, J. F.; Elder, S. H.; Zaban, A.; Borse, P. H.; Kulkarni, S. K.; Doran, G. S.; Whitfield, H. J. *Proc. Natl. Acad. Sci.* **2002**, *99* [Suppl. 2], 6476.
(22) Pitcher, M. W.; Ushakov, S. V.; Navrotsky, A.; Woodfield, B. F.; Li, G.; Boerio-Goates, J.; Tissue, B. M. *J. Am. Ceram. Soc.* **2004**, *36*, 857.
(23) Wang, L.; Navrotsky, A.; Stevens, R.; Woodfield, B. F.; Boerio-Goates, J. *J. Chem. Thermodyn.* **2003**, *35*, 1151.
(24) Stevens, R.; Boerio-Goates, J. *J. Chem. Thermodyn.* **2004**, in press.
(25) Lashley, J. C.; Lang, B. E.; Boerio-Goates, J.; Woodfield B. F. *J. Chem. Thermodyn.* **2002**, *34*, 251.
(26) Rupp, J.; Birringer, R. *Phys. Rev. B* **1987**, *36*, 7888.
(27) Chen, Y. Y.; Yao, Y. D.; Hsiao, S. S.; Jen, S. U.; Lin, B. T.; Lin, H. M.; Tung, C. Y. *Phys. Rev. B* **1995**, *52*, 9364.
(28) Zhang, H.; Banfield, J. F. *J. Mater. Chem.* **1998**, *8*, 2073.
(29) Zhang, H.; Banfield, J. F. *Nanostruct. Mater.* **1998**, *10*, 185.
(30) Volokitin, Y.; Sinzig, J.; de Jongh, L. J.; Schmid, G.; Vargaftik, M. N.; Moiseev, I. I. *Nature* **1996**, *384*, 621.
(31) JADE 6.0, Materials Data Incorporated: Livermore, California, 1995.

Table 1. Crystallite Sizes from XRD, Surface Areas from BET, and Solution Enthalpies of CoO Nanoparticles in HCl (5.0 N) Solvent at 25.00 °C[a]

sample designation[b]	particle size[c] (nm)	surface area[d] ($m^2 \cdot mol^{-1}$)	solution enthalpy: measured[e] ($kJ \cdot mol^{-1}$)	solution enthalpy: corrected for impurities[f] ($kJ \cdot mol^{-1}$)
C350	7.0 ± 1.0	8920.7 ± 28.2	−112.27 ± 2.80	−133.16 ± 3.32
C400	12.9 ± 1.6	5745.1 ± 25.5	−104.01 ± 2.53	−124.10 ± 3.02
C450	16.5 ± 0.9	4451.7 ± 21.7	−111.18 ± 3.08	−117.00 ± 3.25
C500	20.9 ± 2.2	3061.7 ± 22.5	−108.87 ± 2.74	−112.84 ± 2.81
CoO[g]	60 μ (bulk)			$-106.84 \pm 0.12^{+??}$

[a] The molecular mass of CoO is 74.9326 $g \cdot mol^{-1}$ and − means the solution enthalpies are exothermic. [b] The sample designation indicates the temperature, in °C, at which the sample was annealed as described in the text. [c] The uncertainty of the particle size is the standard deviation of the mean from the widths of all the peaks. [d] The uncertainty is the standard deviation of 5 points from BET measurement. [e] The samples were assumed to be pure CoO. The uncertainty is the standard deviation of 5 runs of each sample. [f] Corrected for H_2O and excess oxygen by treating H_2O as bulk liquid water and assuming that the excess oxygen was present in the sample as Co_3O_4. [g] Details of the experiments on bulk CoO have been reported.[25]

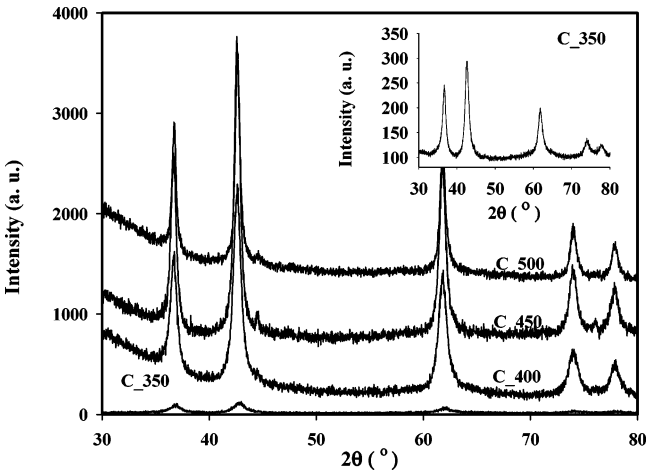

Figure 1. XRD patterns of CoO nanoparticles. The samples were obtained at 350, 400, 450, and 500 °C, respectively. The insert is an expanded scale pattern of the sample obtained at 350 °C.

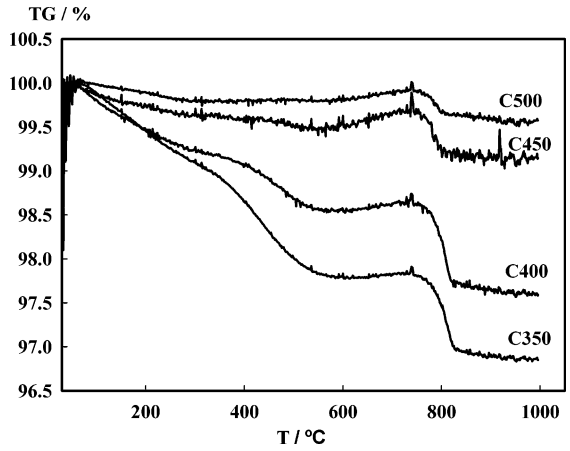

Figure 2. Thermogravimetry scans of samples.

particles shown in Figure 1 indicate that all of the samples are of the rocksalt structure. The crystallite sizes, calculated using the refinement/whole profile fitting (WPF) with Jade 6.0 software,[31] are listed in Table 1. None of the peaks from the starting materials are present in the XRD patterns of the nanoparticles. Several additional, low-intensity peaks were observed in the patterns of samples C450 and C500; these are attributed to Co_3O_4 (PDF# 62-9976). While peaks attributed to Co_3O_4 are not apparent in the patterns of C350 and C400, this impurity is detected from the TG studies discussed below.

In the thermogravimetric experiments, the samples showed a continual weight loss below 600 °C and a stepwise weight loss at 800 °C as shown in Figure 2. The first weight loss is associated with the evolution of water from the surface of the nanoparticles, while the second is attributed to the decomposition of a Co_3O_4 impurity according to the reaction $Co_3O_4 = 3\ CoO + {}^1/_2\ O_2(g)$. This latter conclusion is based on the decomposition behavior of Co_3O_4[32] and a report that excess oxygen on CoO is localized on the surface of nanoparticles as Co_3O_4.[11] From the magnitudes of the respective weight losses, the amounts of adsorbed water and excess oxygen were calculated first giving a formula $CoO_x \cdot (H_2O)_y$, and then as $CoO \cdot (H_2O)_y \cdot (Co_3O_4)_z$ (see Table 2). No metal impurities were detected by electron microprobe analysis.

The surface areas measured by BET are listed in Table 1. The particle sizes calculated from the BET specific surface areas are very close to the crystallite sizes determined from the XRD patterns, but smaller than those measured from TEM and SEM images (Figure 3). This might suggest a slight aggregation of the particles. The bulk and 7-nm particles showed X-ray diffraction peaks at very similar positions, implying no significant shift in lattice parameter with particle size. Only a broad peak associated with adsorbed water was found in the IR spectra of the nanoparticles. No evidence for hydroxyl formation distinct from physisorption of H_2O was observed. The low temperature of water loss is consistent with weakly bound water.

However, a full statistical analysis of particle size distribution observed by electron microscopy was not attempted. The BET surface area was used in the surface enthalpy calculations, as has been done in our previous studies on Al_2O_3,[20] TiO_2,[21] and ZrO_2.[22]

Surface Enthalpy. The measured enthalpies of solution are listed in Table 1, both before and after correction for the water and Co_3O_4 impurities. On an atomic level, the dissolution process destroys all the bonds within the solid, replacing them with ion−solvent interactions. The difference between the enthalpy of solution of nanoparticles and of bulk sample is thus the sum of all the energy differences between the two samples. For the present investigation, we assume that

(32) Chen, M.; Hallstedt, B.; Gauckler, L. *J. Phase Equilib.* **2003**, *24*, 212.

Table 2. CoO Nanoparticle Composition as Determined by Thermogravimetric Analysis

sample[a]	H_2O (wt %)[b]	oxygen (wt %)[b]	molar ratio	phase composition
C350	2.18 ± 0.04	0.90 ± 0.02	$CoO_{(1.043\pm0.001)}\cdot(0.094 \pm 0.002)H_2O$	$CoO\cdot(Co_3O_4)_{0.050}\cdot(H_2O)_{0.12}$
C400	1.44 ± 0.03	0.98 ± 0.03	$CoO_{(1.047\pm0.001)}\cdot(0.061 \pm 0.002)H_2O$	$CoO\cdot(Co_3O_4)_{0.015}\cdot(H_2O)_{0.06}$
C450	0.46 ± 0.06	0.30 ± 0.02	$CoO_{(1.014\pm0.001)}\cdot(0.019 \pm 0.002)H_2O$	$CoO\cdot(Co_3O_4)_{0.015}\cdot(H_2O)_{0.02}$
C500	0.19 ± 0.02	0.22 ± 0.01	$CoO_{(1.010\pm0.001)}\cdot(0.008 \pm 0.001)H_2O$	$CoO\cdot(Co_3O_4)_{0.010}\cdot(H_2O)_{0.01}$

[a] The sample designation indicates the temperature, in °C, at which the sample was annealed, as described in the text. [b] The uncertainties are two standard deviations of the mean of 5 measurements of each sample.

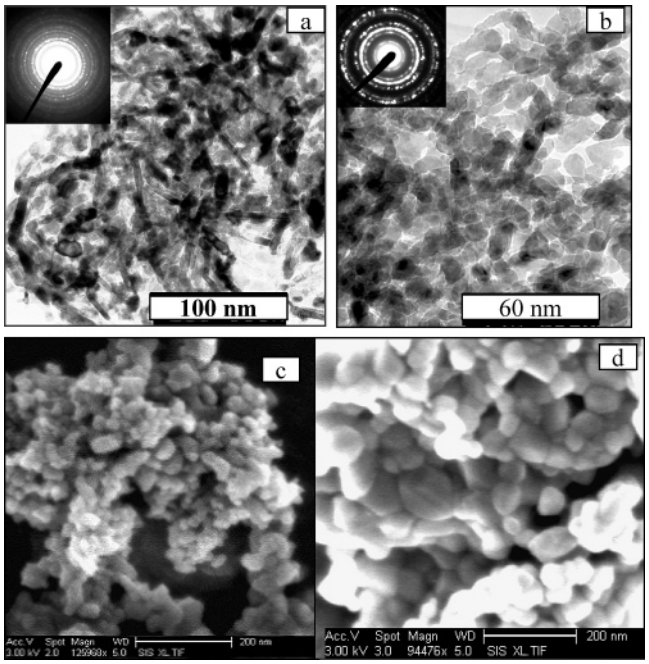

Figure 3. TEM (a and b) and SEM (c and d) images: a, b, c and d are samples obtained at 350, 400, 450, and 500 °C, respectively..

the measured enthalpy difference arises from the surface enthalpy and the presence of water and Co_3O_4. The water present in the samples is taken to be energetically equivalent to bulk liquid water, just as we have done in the previous studies of nanocrystalline titania[21] and zirconia.[22] The dilution enthalpy of bulk H_2O in 5.0 N HCl acid and the heat content due to the slight temperature difference between the laboratory and the solvent in the calorimeter are less than 0.1% of the total measured heat and are neglected. There was no obvious heat detected when a pellet of pure Co_3O_4 was dropped from room temperature into 5.0 N HCl in the calorimeter. This suggests that Co_3O_4 is very slow to dissolve. Therefore, the correction for Co_3O_4 simply represents an adjustment of the sample masses to that of the CoO present in a pellet.

The excess enthalpies of the CoO nanoparticles with respect to CoO bulk were calculated from

$$\Delta H^{ex} = \Delta H_{s(bulk)} - \Delta H_{s(nano)} \quad (2)$$

where $\Delta H_{s(bulk)}$ and $\Delta H_{s(nano)}$ were measured directly. The excess enthalpy of nanoparticles relative to bulk can be considered to arise from the increased surface area and expressed as

$$\Delta H^{ex} = \Delta H_{surface}\cdot A \quad (3)$$

where $\Delta H_{surface}$ is the surface enthalpy and A is the surface area. Thus, as shown in Figure 4, by plotting

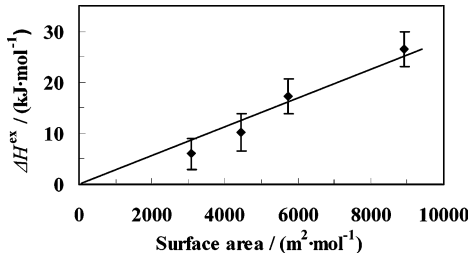

Figure 4. Excess enthalpies versus BET surface area of CoO nanoparticles. The slope is the surface enthalpy, 2.82 ± 0.20 J·m^{-2}.

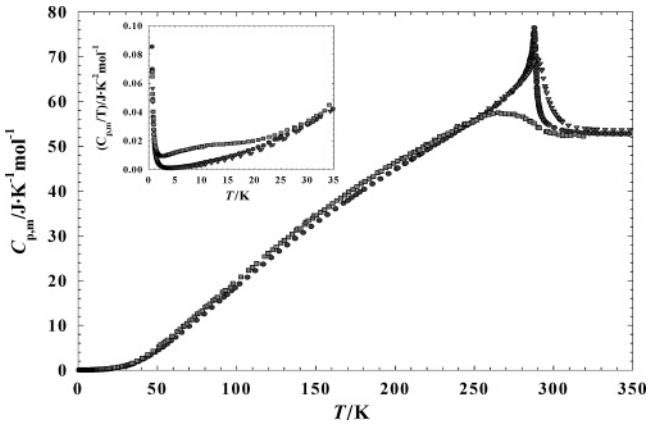

Figure 5. Heat capacity versus temperature curves of CoO samples: ■ 7 nm; ▼ 60 μm; and ★ single crystal. The inset plots the low-temperature data as $C_{p,m}/T$ versus T using the same symbols.

excess enthalpy versus the surface area determined by BET, $\Delta H_{surface} = 2.82 \pm 0.20$ J·m^{-2} was obtained. The uncertainty of 0.2 J·m^{-2} includes the uncertainty of the calorimetric measurements and of the masses of H_2O and Co_3O_4 impurity.

Excess Heat Capacity and Surface Entropy. The molar heat capacity $C_{p,m}$ of sample C350, which had been prepared at 350 °C and found to have a particle size of 7.0 ± 1.0 nm and chemical composition of $CoO_{(1.043\pm0.001)}\cdot(0.094\pm0.002)H_2O$, was measured from 0.6 to 320 K. To calculate the evolution of the excess entropy of the nanoparticles with temperature, heat capacities of 60-μm CoO particles and large (~3 mm × 3 mm × 1 mm) chunks of a single crystal were measured with the same apparatus. The experimental data are shown in Figure 5. The $C_{p,m}$ of the single crystal showed a sharply peaked anomaly with a maximum at 288.78 K; the anomaly for the 60 μm particles is broader but at a slightly higher temperature, 289.40 K; only the results in the vicinity of the transition are shown for this sample. As described earlier, one can consider the composition of the sample in two ways, $CoO_{1.043}$ plus adsorbed water, or CoO plus an impurity of Co_3O_4 and water. We have calculated the molar heat capacity of the nanoparticles two ways. First, we used the molec-

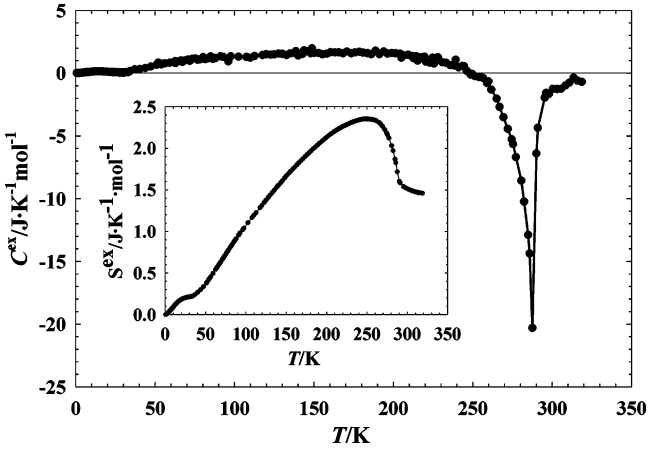

Figure 6. Excess heat capacity of CoO nanoparticles relative to the single crystal as a function of temperature. The inset is the excess entropy.

ular weight for $CoO_{1.043}$ and corrected for water. The second calculation corrected for Co_3O_4 as a separate phase and for water. The water heat capacities used in the correction were based on literature results for bulk ice (Ih)[33−35] to which a series of Debye and Einstein functions were fitted to reproduce the literature results and extrapolated above 270 K. The heat capacity for the Co_3O_4 corrections were based on those reported for bulk cubic Co_3O_4[36] but taking only an estimate of the lattice heat capacity near 30 K where Co_3O_4 has a magnetic transition.

The nanoparticle heat capacity, corrected only for water, is lower than that of the larger particles above 100 K, a result that seems unlikely given the expectation that the lattice vibrations of the nanoparticles should be softer and surface contributions more significant than those of the bulk. Since Co_3O_4 has been reported to form on the surface of CoO nanoparticles,[11] the second assumption about the excess oxygen content is probably a better representation of the real phase composition of the particles. Applying corrections for both water and Co_3O_4 yields the results in Table 3 Figure 5. This nanoparticle curve lies above that for the large particles everywhere except in the magnetic transition region. The inset to Figure 5 shows the low-temperature data plotted as $C_{p,m}/T$ vs T, so that the differences can be seen more clearly. Taking the single crystal as the baseline, we obtain the excess heat capacity as $C^{ex} = C_{(nano)} - C_{(single\ crystal)}$ (see Figure 6). Integrating $\int_0^T (C^{ex}/T)dT$ yields the excess entropy $\Delta_0^T S^{ex}$ relative to CoO single crystal; this is given as an inset to Figure 6. $\Delta_0^T S^{ex}$ generally increases with temperature until 245 K. As the magnetic entropy in the single-crystal begins to evolve, $\Delta_0^T S^{ex}$ diminishes, dropping to 1.5 ± 0.3 J·K^{-1}·mol^{-1} at 298 K from the maximum of 2.4 ± 0.3 J·K^{-1}·mol^{-1}at 245 K. The small bump visible in S^{ex} near 20 K is attributed to the magnetic transition in Co_3O_4. By correcting for the lattice contributions of bulk Co_3O_4, the small broad anomaly below 30 K in the experimental C_p becomes more evident. The error associated with S^{ex} includes estimates of uncertainties arising from the corrections for Co_3O_4 and H_2O.

Using the surface area determined for the C350 particles by BET, we can calculate a surface excess entropy. At 245 K, we get 2.8 ± 0.3 mJ·K^{-1}·m^{-2} and at 298 K we get 1.5 ± 0.3 mJ·K^{-1}·m^{-2}. It is interesting to compare these with the only other reported excess entropy of which we are aware, the result of Jura and Garland for MgO.[37] They report 2.8 mJ·K^{-1}·m^{-2} at 298 K, a value that is in (possibly fortuitously) excellent agreement with our result at 245 K, before the magnetic interactions begin to diminish the excess entropy.

Surface Gibbs Free Energy. The excess Gibbs free energy at 298 K calculated from surface enthalpy and $\Delta_0^{298} S^{ex}$ using eq 1 is 2.77 ± 0.28 J·m^{-2}. However, $\Delta_0^{298} S^{ex}$ includes the contributions of both surface and magnetic effects. It is reasonable to assume that $\Delta_0^{245} S^{ex}$ represents a typical surface entropy, especially given the agreement with the MgO result. Using it gives a surface Gibbs free energy of 2.74 ± 0.28 J·m^{-2}. On the basis of the above calculations, the contribution of the surface entropy term is about 3%, and one can conclude that the surface enthalpy term dominates the surface energy of the CoO nanoparticles as expected.[19]

Excess Entropy of Magnetic Transition. As shown in Figure 5, the excess heat capacity begins to decrease at 245 K when the sharp magnetic transition associated with long-range order of the Co^{2+} spins in the single crystal dominates the excess heat capacity. The excess entropy of magnetic transition ΔS_{mag}^{ex} of nanoparticles relative to single crystal can be calculated from

$$\int \Delta S_{mag}^{ex} = \int_0^T C_{mag}^{ex}/TdT/T \qquad (4)$$

where $C_{mag}^{ex} = C^{ex} - C_{lat}^{ex}$ if one can estimate the excess lattice contribution, C_{lat}^{ex}. We have made assumptions at two limiting scenarios to get a measure of C_{mag}^{ex}. First, if we assume that C_{lat}^{ex} can be neglected relative to C_{mag}^{ex} in the magnetic transition range from 200 to 310 K, and that C_{mag}^{ex} is negligibly small below 200 K, we find that $\Delta S_{mag}^{ex} = -0.8 \pm 0.3$ J·K^{-1}·mol^{-1}. With the other approach, we extrapolate the behavior of C^{ex} from 50 to 200 K in a linear fashion to 310 K and use the extrapolated values as an estimate of C_{lat}^{ex}. This yields $\Delta S_{mag}^{ex} = -1.6 \pm 0.5$ J·K^{-1}·mol^{-1}. In both cases, the excess magnetic entropy is negative.

Generally, the entropy of the magnetic transition that develops below T_N is associated with long-range ordering of the magnetic spins. Another signature of long-range order is the sharp peak in the heat capacity at T_N, often referred to as a λ-transition. The negative value of ΔS_{mag}^{ex} in this investigation indicates that long-range ordering is significantly diminished in the nanoparticles. This conclusion is supported by the gradual rounding of the heat capacity peak as one goes from large single crystals where extensive long-range order is possible, to the 60 μm particles, and then to the nanoparticles. We estimate that the nanoparticles con-

(33) Flubacher, P.; Leadbetter, A. J.; Morrison, J. A. *J. Chem. Phys.* **1960**, *33*, 1751−1755.
(34) Giauque, W. F.; Stout, J. W. J. *Am. Chem. Soc.* **1936**, *58*, 1144−1150.
(35) Haida, O.; Matsuo, T.; Suga, H.; Seki, S. *J. Chem. Thermodyn.* **1974**, *6*, 815−825.
(36) Khriplovich, L. M.; Kholopov, E. V.; Paukov, I. E. *J. Chem. Thermodyn*. **1982**, *14*, 207−217.
(37) Jura, G.; Garland, C. W. *J. Am. Chem. Soc.* **1952**, *74*, 6033−6034.

Table 3. Standard Entropy of CoO Nanoparticles at 298 K Without and With H_2O and Co_3O_4 Corrections

composition	${}_0^{298.15}S_m^0$ $J \cdot K^{-1} \cdot mol^{-1}$	$\Delta_0^{298.15}S^{ex}$ $J \cdot K^{-1} \cdot mol^{-1}$ [a]	$T\Delta_0^{298.5}S^{ex}$ $J \cdot m^{2}$ [b]	
$CoO_x \cdot yH_2O$ [c]	55.1 ± 0.2 [d]	2.9 ± 0.2	0.09 ± 0.01	without corr.
$CoO_x \cdot yH_2O$	51.2 ± 0.2	-1.0 ± 0.2	-0.03 ± 0.01	corr. H_2O, HF[g]
$CoO \cdot xCo_3O_4 \cdot yH_2O$ [e]	53.7 ± 0.3 [f]	1.5 ± 0.3	0.05 ± 0.01	corr. H_2O, Co_3O_4, HF[g]
CoO bulk	52.8 ± 0.1			

[a] $\Delta_0^{298.15}S^{ex} = \Delta_0^{298.15}S^0_{m(nano)} - \Delta_0^{298.15}S^0_{m(SingleCrystal)}$; where $\Delta_0^{298.15}S^0_{m(SingleCrystal)} = (52.2 \pm 0.1)\ J \cdot K^{-1} \cdot mol^{-1}$. [b] The surface area from BET measurement is 8917.0 $m^2 \cdot mol^{-1}$. [c] $x = 1.043 \pm 0.001$; $y = 0.094 \pm 0.002$, mole mass is 77.3140 $g \cdot mol^{-1}$. [d] The error is estimated from the overall heat capacity measurement. [e] $x = 0.050 \pm 0.001$; $y = 0.121 \pm 0.002$; molar mass is 89.1515 $g \cdot mol^{-1}$. [f] Errors include the uncertainties of Co_3O_4 and H_2O contents. [g] Correction for upturn in Cp at very low T due to HF (hyperfine) splittings.

tain no more than 16 unit cells on an edge; this sets an upper limit to the length scale of the magnetic interaction unless interactions extend across grain boundaries. We note that by 200 K there is likely a significant population of the two lowest excited Co^{2+} crystal field states arising from the ^4F ground state of the free ion. If one neglects the lattice heat capacity contribution, the Schottky contribution arising from the thermal population of these excited states should cancel out in the calculation. To the extent that the crystal field levels are different in the nanoparticles, what we are calling ΔS^{ex}_{mag} may in fact contain a small contribution due to the single-ion electronic excitations.

This diminished magnetic entropy in CoO nanoparticles is consistent with previously published low-temperature calorimetric results on zinc ferrite nanoparticles.[38] Of course the separation of excess entropy into contributions from a surface vibrational term and the effects of the magnetic transition is only an approximation. Magnetic susceptibilities measured on CoO nanoparticles[39] show no significant change in the Néel temperature from that of bulk CoO. However, as the temperature decreases below 100 K, the susceptibility begins to increase, a result that is attributed to the interaction of uncompensated spins on the surface. If we assume that the number of such spins is still small compared to the number of ions that are interacting on the interior of the particle then the contribution of such spins to the heat capacity is small compared to that from the long-range cooperative ordering at 265 K. Thus, it is reasonable to break up the contributions as we have done.

Debye Temperature, Internal Magnetic Field, and Low-Temperature Heat Capacity Linear Term. The heat capacity at low temperature can be analyzed to yield three parameters that further characterize the differences between nanoparticles and macroparticles. These are the Debye temperature Θ_D, which gives a measure of the energy of the lattice vibrations, the strength of the internal magnetic field H around the Co nucleus, which splits nuclear levels and gives rise to the upturn in C_p that is evident below 1 K in Figure 4, and the magnitude of a heat capacity contribution that is linear in T. The function

$$C = aT^{-2} + dT + eT^3 \qquad (5)$$

was fitted to the corrected heat capacity of both the nanoparticles and the single crystals.

Table 4. Parameters Extracted from Low Temperature Heat Capacity of CoO

material	H Tesla	linear term $mJ\ K^{-2}\ mol^{-1}$	Θ_D K
single crystal	46.1 ± 0.5	0.4 ± 0.1	518 ± 30
7 nm	43.5 ± 1.0	6.0 ± 0.2	225 ± 60

The T^{-2} term represents the contribution from the thermal occupation of the nuclear levels split by the hyperfine interaction due to an internal field, H, while the cubic term models the Debye-low-temperature limiting behavior of the lattice. The a coefficient is related to the hyperfine field as $H = \sqrt{a(mJ \cdot K \cdot mol^{-1})/0.0102(mJ \cdot K \cdot T^{-2} \cdot mol^{-1})}$ where the denominator comes from a collection of constants including the nuclear spin, taken as $^7/_2$ for the Co-59 nucleus. The linear term is usually associated with metals and glasses with $d \approx 10^{-3}\ J \cdot K^{-2} \cdot mol^{-1}$, but it has also been observed in binary oxides with $d \approx 10^{-4}$ to $10^{-5}\ J \cdot K^{-2} \cdot mol^{-1}$ where it is attributed to defects. The results of the analyses are given in Table 4 and from them we gain the following insights. The observation that the CoO nanoparticle C_p shows a linear term comparable to those of glasses suggests either a significant degree of disorder in the nanoparticles or the presence of an amorphous component in the sample. The existence of a linear term has been observed in computer simulations, phonon theory, and heat capacity measurements of nanocrystalline Pd.[40−43] The lower field, H, in CoO nanoparticles indicates a decrease in the coupling between the electronic and nuclear spins. Mössbauer investigations on γ-Fe_2O_3[44] and $BaFe_{12}O_{19}$[45] nanoparticles have also reported such reductions. The origin of the diminished value of H in small particles is a subject of much interest, with attributions ranging from the increased influence of surface ions which have a smaller H[41] to the existence of fluctuations in the magnetization direction.[46] The greatly reduced Debye temperature of the nanoparticles indicates a softening of the phonons in the nanoparticles compared to those in the single crystal.

Conclusions

CoO nanoparticles were synthesized by precipitation and thermal decomposition in an H_2/Ar atmosphere. The

(38) Ho, J. C.; Hamdeh, H. H.; Chen, Y. Y.; Lin, S. H.; Yao, Y. D.; Willy, R. J.; Oliver, S. A. *Phys. Rev. B* **1995**, *52*, 10122.
(39) Zhang, L.; Xue, D.; Gao, C. *J. Magn. Magn. Mater.* **2003**, *267*, 111.
(40) Smith, J. R. *Phys. Rev. Lett.* **1993**, *70*, 2774.
(41) Wolf, D.; Wang, J.; Phillpot, S. R.; Gleiter, H. *Phys. Rev. Lett.* **1995**, *74*, 4686.
(42) Shrivastava, K. N. *Nano Lett.* **2002**, *2*, 21.
(43) Oya, H. *J. Phys. Soc. Jpn.* **1999**, *68*, 3916.
(44) Haneda, K.; Morrish, A. H. *Phys. Lett.* **1977**, *64A*, 259.
(45) Gajbhiye, N. S.; Vijayalakshmi, A. *Mater. Trans., JIM* **1999**, *40*, 1084.
(46) Haneda, K. *Can. J. Phys.* **1987**, *65*, 1234.

surface enthalpy, 2.8 ± 0.2 J·m^{-2}, was determined using solution calorimetry with a HCl acid solvent at 25.00 °C. Heat capacity measurements performed on nanoparticles, using adiabatic and semi-adiabatic calorimeters, revealed several differences from the bulk, including a rounded maximum in the heat capacity at 265 K, a reduction of the Néel temperature by 23 K from the single crystals, a large linear term at low temperatures, a reduced hyperfine field, and a reduced Debye temperature. The excess entropy obtained from the excess heat capacities relative to CoO single crystal was a maximum 2.4 ± 0.3 J·K^{-1}·mol^{-1} at 245 K with the value dropping to 1.5 ± 0.3 J·K^{-1}·mol^{-1} at 298 K. The surface entropy term is estimated to contribute only about 3% to the surface Gibbs free energy at 298 K. Assuming the magnetic effects predominate between 200 and 310 K, the excess entropy of the magnetic transition is -0.8 ± 0.3 J·mol^{-1}. The negative ΔS_{mag}^{ex} implies that much of the long-range order is lost in nanoparticles.

Acknowledgment. TEM imaging was performed at the National Center for Electron Microscopy, Lawrence Berkeley National Laboratory. We thank S. V. Ushakov and M. Wang at UC Davis for the help on TEM and SEM, and T. Walker, S. Doot, and B. Lang at BYU for assistance with the heat capacity measurements. This work was supported by the U.S. Department of Energy (DOE) under Grant DEFG0301ER1S237.

CM049040I